

---

**I.A. Drabkin<sup>1</sup>, V.B. Osvenski<sup>1</sup>, Yu.N. Parkhomenko<sup>1</sup>, A.I. Sorokin<sup>1</sup>,  
G.I. Pivovarov<sup>2</sup>, L.P. Bulat<sup>3</sup>**

<sup>1</sup>State Scientific-Research and Design Institute of Rare-Metal Industry “Giredmet” JSC,  
5/1, B. Tolmachevsky lane, Moscow, 119017, Russia;

<sup>2</sup>Technological Institute of Superhard and New Carbon Materials “Tisnum”,  
7 a, Centralnaya Str., Troitsk, Moscow, 142190, Russia;

<sup>3</sup>The National Research University ITMO, 49, Kronverkskiy Ave.,  
Saint-Petersburg, 197101, Russia

## **ANISOTROPY OF THERMOELECTRIC PROPERTIES OF P-TYPE NANOSTRUCTURED MATERIAL BASED ON $(Bi, Sb)_2Te_3$**

---

*Anisotropy of thermoelectric properties of nanostructured  $Bi_{0.4}Sb_{1.6}Te_3$ , material obtained by spark plasma sintering (SPS) method in the temperature range of 245 to 420 K has been investigated. It has been established that anisotropy value is increased with sintering pressure increase and temperature reduction. Electric conductivity anisotropy coefficient is higher than thermal conductivity anisotropy coefficient. Based on the experimental values of electric and thermal conductivity in different directions, texture coefficients in compacted material have been calculated. The resulting calculated temperature dependences of thermoEMF are in reasonable agreement with the experimental data. The results of calculation of temperature dependence of lattice thermal conductivity in perpendicular and parallel directions with respect to trigonal axis are given for a single-crystal grain in the extrinsic conduction region. Starting from some temperature depending on sample manufacturing conditions, the value of thermoelectric figure of merit  $ZT$  in a direction parallel to compaction axis, becomes higher than in a perpendicular direction, which is due to the emergence of minor carriers and the difference in the values of hole-electron mobility ratios in single-crystal material for parallel and perpendicular directions with respect to trigonal axis. Comparison of errors in determination of material thermoelectric parameters with Harman's method and the method of separate measurement of electric conductivity, thermoEMF and thermal conductivity on different samples has been made. In the latter case measurement of electric and thermal conductivity without regard to anisotropy can yield overrated  $ZT$  values.*

**Key words:** nanostructured material, anisotropy coefficient, electric conductivity, thermal conductivity.

### **Introduction**

The  $Bi_2Te_3$  compound and solid solutions on its basis possess a layered crystalline structure with monoatomic layers alternating as  $Te^{(1)} - Bi - Te^{(2)} - Bi - Te^{(1)}$  in the  $c$  direction. These quintet layers are interconnected by weak Van der Waals bonds. Such anisotropic structure defines possible anisotropy of thermoelectric properties along and across the layers. In a bulk polycrystalline sample the anisotropy of properties is the stronger, the higher is texture degree, i.e. preferred crystallographic orientation of grains.

It is well known that single crystals and polycrystals obtained by methods of oriented

crystallization of the melt (for instance, zone melting) or extrusion, possess 100-percent or so texture and, as a consequence, pronounced anisotropy of thermoelectric properties. In polycrystalline material obtained by hot pressing of powders, the possibility of texture origination and anisotropy of thermoelectric properties increases with increasing grain size. Starting from work [1] where for the first time the bulk nanostructured material with high thermoelectric properties ( $ZT = 1.4$ ) was obtained, it has been believed that samples with randomly oriented nanosize grains are isotropic. Therefore, in the majority of subsequent works that reported on obtaining *p*-type material with high  $ZT$  values the possibility of thermoelectric properties anisotropy was ignored.

However, a more thorough and purposeful investigation based on the measurement of thermoelectric properties in perpendicular and parallel directions with respect to compaction axis, revealed electric and thermal conductivity anisotropy of compacted material based on  $Bi_2Te_3$ , including that produced from nanopowders. Anisotropy due to the presence of texture is more pronounced in *n*-type material [2].

Anisotropy value, characterized by anisotropy coefficient, depends on a combination of factors: solid solution composition [3], morphology of source powder particles [4], as well as compaction conditions, namely pressure and temperature. This accounts for a quantitative difference in anisotropy coefficients observed in the samples produced under different conditions.

In the present work, anisotropy of thermoelectric properties of *p*-type nanostructured  $Bi_{0.4}Sb_{1.6}Te_3$  material obtained by spark plasma sintering (SPS) has been studied as a function of compaction temperature and pressure. Unlike the majority of works, electric conductivity, thermoEMF, thermal conductivity and thermoelectric figure of merit were determined by two methods: Harman's method of measurement on the same sample and method of separate measurement of electric conductivity, thermoEMF, thermal conductivity on different samples.

## **Experimental procedure**

Nanostructured samples were obtained from nanopowders of synthesized material of given composition. As a source raw material, *Bi* (99.999), *Sb* (99.999), *Te* (99.999) was used. Synthesis was performed by direct alloying of components in sealed quartz ampoules. The resulting ingots were subject to mechano-activated treatment in protective atmosphere in high-energy planetary ball mill PM 400 (Retsch, Germany). Compact nanostructured material samples of composition  $Bi_{0.4}Sb_{1.6}Te_3$  were obtained by SPS method in SPS-511S installation (SPS Syntex, Japan). This method offers a number of advantages over conventional hot-pressing technique [5]. Cold-pressed pellet, preliminarily produced from nanopowder, was transferred to SPS installation. All operations with nanopowder were carried out in a glove box in protective atmosphere with moisture content  $O_2$  control. Concentration of  $O_2$  was maintained below 10 ppm to prevent from powder oxidation.

Samples sintered in graphite mold were as thick as 3 to 10 mm with diameter 20 mm. Sintering was made at temperatures 450 and 500 °C under a pressure of 30 and 50 MPa during 5 minutes. From the resulting pellets on electric erosion cutting machine APTA-151 (Delta-Test, Russia) samples of different size were cut depending on the method of properties measurement.

Thermoelectric properties of the bulk nanostructured material were measured by two methods.

In the temperature range of 245 to 355 K measurements were made by six-wire Harman's method [6] on the samples of size  $2.5 \times 2.5 \times 4$  mm<sup>3</sup>. The specific feature of this method is that thermoelectric figure of merit  $Z$ , thermoEMF  $\alpha$  and electric conductivity  $\sigma$  are determined by direct measurement on the same sample, and thermal conductivity  $\kappa$  is calculated from the formula

$Z = \alpha^2 \sigma / \kappa$ . In so doing, electric and thermal conductivity is measured in one direction, perpendicular or parallel to compaction axis.

Account of thermal losses due to heat fluxes through sample input leads and heat radiation from the sample and the leads allows reducing considerably the errors of  $Z$  measurement. The calculated values of proper corrections are given in [7]. The accuracy of  $Z$  determination by Harman's method is much higher as compared to separate measurement of  $\alpha$ ,  $\sigma$  and  $\kappa$ , since it is a quotient of electrical voltages obtained in the course of experiment. The advantage of Harman's method is independence of results on sample shape and possibility of measurements on small-size samples. The shortcoming of Harman's method is the presence of soldered electric contacts to sample which automatically adds contact resistances to sample resistance.

Measurements were made on automated bench (Giredmet, Russia) and installation DX-8080 (RMT, Russia). According to our estimates, with Harman's method the measurement errors are: thermoEMF  $\pm 1.5\%$ , electric conductivity  $\pm 2\%$ , thermoelectric figure of merit  $\pm 3\%$ , thermal conductivity determined by calculation  $\pm 5\%$ .

The temperature dependences of thermoelectric properties in the range of temperatures 300 to 420 K were also determined by separate measurement of electric conductivity, thermoEMF and thermal conductivity on different samples with subsequent calculation of thermoelectric figure of merit. Practically all the results reported in foreign works on thermoelectricity of recent years have been obtained by this method which employs standard equipment. Electric conductivity and thermoEMF were measured on ZEM 3 installation (Ulvac, Japan) on the samples of size  $2.5 \times 2.5 \times 10 \text{ mm}^3$ . Thermal conductivity was calculated by the formula  $\kappa = D_t \times C_p \times d$ , where  $D_t$  – temperature diffusivity,  $C_p$  – specific heat,  $d$  – density. Each of these parameters is measured on different samples, which increases the error in measuring  $\kappa$  and, hence,  $Z$ . Temperature diffusivity was measured by laser flash method on LFA 457 installation (Netzsch, Germany). Specific heat was measured by calorimetric method on the samples of size  $0.7 \times 2 \times 4 \text{ mm}^3$  on DSC-404C installation (Netzsch, Germany). The density of samples was measured by Archimedes's method.

According to our estimates, with separate measurement of  $\alpha$ ,  $\sigma$  and  $\kappa$ , the errors are as follows: thermoEMF  $\pm 7\%$ , electric conductivity  $\pm 4\%$ , thermal conductivity  $\pm 12\%$  (with regard to errors in measuring  $D_t$ ,  $C_p$  and  $d$ ), thermoelectric figure of merit – minimum  $\pm 20\%$ .

Note that with said method the relatively high error in measuring  $\sigma$  and  $\alpha$  is primarily related to low accuracy of fixing the distance between thermocouples that simultaneously serve as probes. When measuring temperature diffusivity by nonstationary laser flash method it is not quite clear to which temperature one should compare the measured value, since heat wave, especially at the initial moment after heat pulse, propagates under conditions of strong overheat with respect to initial sample temperature. Besides, when measuring on samples pressed from powders with high anisotropy of thermal properties, heat wave propagates in conformity with local thermal resistance, rather than over the shortest distance. It may affect the time of heat wave propagation and the measured temperature diffusivity value.

Thus, the above measurement accuracies are permissible for studying temperature dependences of  $\alpha$ ,  $\sigma$  and  $\kappa$ , but give rather approximate estimate of thermoelectric figure of merit.

To determine anisotropy value of thermoelectric properties at different temperatures, measurements by both methods were performed in perpendicular and parallel directions with respect to sample compaction axis.

## Experimental results and discussion

Compacted polycrystalline material formed by anisotropic crystals is locally inhomogeneous, since its constituent single-crystal grains are of different orientation. Any electrical measurement on such material will yield certain effective values of measured quantities. Anisotropy coefficient of the effective electric conductivity  $K_{ep\sigma}$  in compacted material will be characterized by the ratio

$$K_{ep\sigma} = \frac{\sigma_{ep\perp}}{\sigma_{ep\parallel}}, \quad (1)$$

where  $\sigma_{ep\parallel}$  – electric conductivity measured along compaction axis, and  $\sigma_{ep\perp}$  – electric conductivity in a transverse direction. In a similar way, the anisotropy of effective thermal conductivity  $K_{ep\kappa}$  can be determined as the ratio of thermal conductivities along and across compaction axis.

Experimental values of electric conductivity and thermal conductivity anisotropy coefficients at room temperature for samples prepared under different SPS conditions are given in Table 1.

The emergence of electric conductivity and thermal conductivity anisotropy in pressed polycrystalline samples is naturally attributable to texture arising during compaction [3, 8]. The degree of texture increases with increase in pressure. However, with a rise in temperature as a result of recrystallization, texture becomes weaker, which leads to reduction of anisotropy coefficients.

Therefore, even in a relatively small range of change in SPS pressure and temperature, there is a tendency toward  $K_{\sigma}$  and  $K_{\kappa}$  increase with pressure increase and temperature reduction. According to this, as follows from the results given in [3], in *p*-type samples produced by SPS method at 380 °C and pressure 50 MPa, at room temperature  $K_{\sigma} = 1.36$ ,  $K_{\kappa} = 1.25$ . In so doing, electric conductivity anisotropy is more pronounced than thermal conductivity anisotropy. This effect is particularly apparent in *n*-type  $Bi_2Te_3$  material produced by SPS method, where electric resistance anisotropy at room temperature is from 1.4 [4] to 1.7 [2].

*Table 1*

*Electric conductivity and thermal conductivity anisotropy coefficients measured by Harman's method in  $Bi_{0.4}Sb_{1.6}Te_3$  samples at room temperature*

SPS conditions			$K_{ep\sigma}$	$t$	$K_{ep\kappa}$	$n \times 10^{-19}$ , cm <sup>-3</sup>
Time, min	Pressure, MPa	Temperature, °C				
5	50	450	1.17 – 1.18	0.20 – 0.21	1.075 – 1.09	1.75
5	30	450	1.13 – 1.145	0.16 – 0.18	1.07 – 1.075	
5	50	500	1.12 – 1.13	0.15 – 0.16	1.05 – 1.07	
5	30	500	1.09 – 1.105	0.11 – 0.13	1.035 – 1.05	1.64

In single-crystal material there is electric conductivity anisotropy along trigonal axis  $\sigma_{p\parallel}$  and in a perpendicular direction  $\sigma_{p\perp}$ . Let us denote electric conductivity anisotropy coefficient in a single crystal as  $K_{p\sigma}$

$$K_{p\sigma} = \frac{\sigma_{p\perp}}{\sigma_{p\parallel}}. \quad (2)$$

For single crystals of composition  $Bi_{0.4}Sb_{1.6}Te_3$   $K_{p\sigma} = 2.5$  [9]. If in compacted polycrystalline

material the distribution of grains orientation takes place completely at random, its properties are homogeneous in all directions. For such materials there are approximate formulae for the calculation of the effective values of electric conductivity, thermal conductivity and the Hall effect [10-13]. However, in the presence of texture in compacted material the anisotropy of electric conductivity effective values is created. For compacted material we will restrict ourselves to a linear approximation and assume

$$\sigma_{ep\perp} = \frac{2\sigma_{p\perp} + \sigma_{p\parallel}}{3} + t \frac{\sigma_{p\perp} - \sigma_{p\parallel}}{3}, \quad (3)$$

$$\sigma_{ep\parallel} = \frac{2\sigma_{p\perp} + \sigma_{p\parallel}}{3} - t \frac{2(\sigma_{p\perp} - \sigma_{p\parallel})}{3}, \quad (4)$$

where  $t$  – texture coefficient in a direction perpendicular to compaction axis. Multiplier 2 before  $\sigma_{p\perp}$  is due to the fact that there are 2 perpendicular directions and one parallel.

In the absence of texture  $t=0$  and  $\sigma_{ep\perp} = \sigma_{ep\parallel} = \frac{2\sigma_{p\perp} + \sigma_{p\parallel}}{3}$ . With a perfect texture (single crystal)  $t=1$  and  $\sigma_{ep\perp} = \sigma_{p\perp}$ , and  $\sigma_{ep\parallel} = \sigma_{p\parallel}$ . In the absence of texture the difference between (3) or (4) and the expression for electric conductivity in the model of effective medium [11] is within the measurement accuracy and makes 3 – 4 % towards overrating of the effective values, i.e. is quite comparable to electric conductivity measurement error. Therefore, one can consider the expressions (3) and (4) suitable for the analysis of properties of compacted polycrystalline material with low texture coefficient values.

Electric conductivity anisotropy coefficient in compacted material is related to properties of single crystal by the ratios obtained from (3) and (4):

$$2\sigma_{ep\perp} + \sigma_{ep\parallel} = 2\sigma_{p\perp} + \sigma_{p\parallel} \quad (5)$$

and

$$\sigma_{ep\perp} - \sigma_{ep\parallel} = t(\sigma_{p\perp} - \sigma_{p\parallel}). \quad (6)$$

Dividing (6) by (5) and using designations (1) and (2) yields

$$t = \frac{(K_{ep\sigma} - 1)(2K_{p\sigma} + 1)}{(2K_{ep\sigma} + 1)(K_{p\sigma} - 1)}. \quad (7)$$

The values of texture coefficient calculated from (7) are listed in Table 1. Increase in pressure from 30 MPa to 50 MPa results in texture coefficient growth by about 0.03 – 0.04, and a rise in sintering temperature from 450 °C to 500 °C to the same increase of  $t$ .

In the model of effective medium the relation between charge carrier concentration and measured Hall coefficient  $R_{eH}$  is given by the expression [12]

$$R_{eH} = \frac{AB_{eH}}{nec}, \quad (8)$$

where  $n$  – charge carrier concentration,  $e$  – electron charge,  $c$  – light velocity,  $A$  – the Hall factor,  $B_{eH}$  – effective anisotropy factor. In the absence of texture the value of  $B_{eH}$  with regard to the values of effective masses can be approximately considered equal to 0.8 [14]. In a single crystal the difference

in anisotropy coefficients for the directions parallel and perpendicular to triad axis is 10 – 15 %. So, it should be expected that with low texture coefficients the difference in the effective anisotropy coefficients for different directions will be small and comparable to measurement error. Therefore, charge carrier concentration was determined from the Hall effect measured at temperature 77 K with regard to  $B_{eH}$ . In the process, the Hall factor  $A$  was considered equal to unity, since at this temperature and charge carrier concentration the degeneracy condition is observed. The values of hole concentration in the investigated samples are listed in Table 1.

Of particular interest is to study the temperature dependence of thermoelectric properties anisotropy. As an example, Fig. 1 shows measured by Harman's method temperature dependences of electric conductivity  $\sigma$ , thermoEMF  $\alpha$ , thermal conductivity  $\kappa$  and thermoelectric figure of merit  $ZT$  for a sample obtained by SPS method at a pressure of 50 MPa and temperature 450 °C, as well as the respective temperature dependences of anisotropy coefficients.

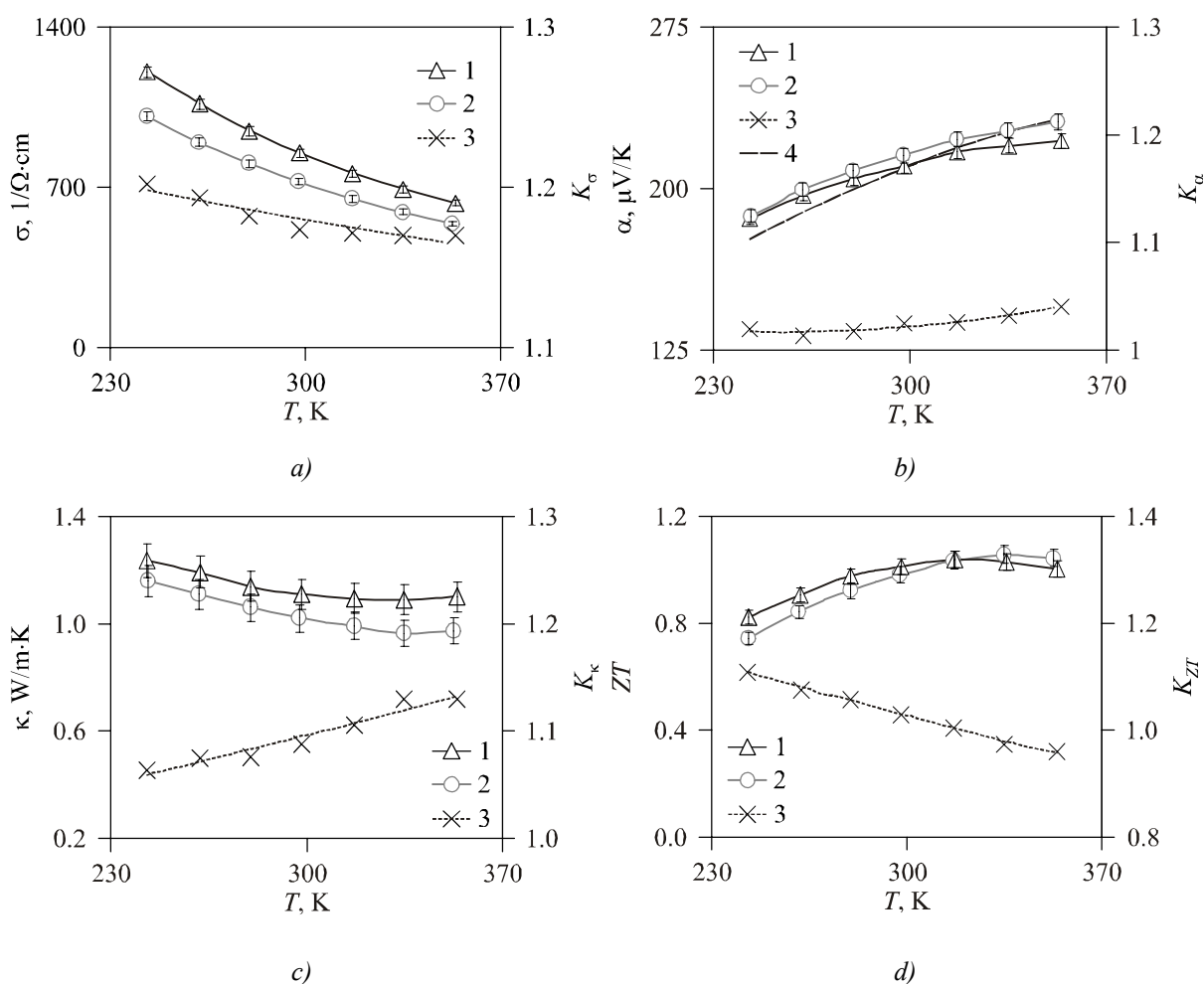


Fig. 1. Temperature dependences of electric conductivity (a), thermoEMF (b), thermal conductivity (c), dimensionless thermoelectric figure of merit (d) of  $\text{Bi}_{0.4}\text{Sb}_{1.6}\text{Te}_3$  samples prepared by SPS method at a pressure of 50 MPa, temperature 450 °C.

Measurement by Harman's method: 1 – perpendicular to compaction axis, 2 – parallel to compaction axis, 3 – anisotropy coefficient, 4 – result of thermoEMF calculation.

The data on electric conductivity, the Hall effect and thermoEMF allow calculating with a knowledge of band parameters the temperature dependences of thermoelectric properties within the framework of parabolic bands and isotropic scattering of charge carriers. The difficulty of

calculation lies in a wide difference between the data on band parameters provided by different authors. Thus, according to [15], the density-of-state effective mass of holes  $m_p$  for composition  $Bi_{0.45}Sb_{1.55}Te_3$  is  $0.43m_e$ , and according to [16] –  $0.968 m_e$ . In our calculation we considered scattering parameter  $r = -0.5$ , which corresponds to acoustic scattering of charge carriers. The density-of-state effective mass was chosen on condition of the best matching between calculated and experimental temperature dependences of thermoEMF. The ratio between hole and electron masses, between hole and electron mobilities, the energy gap width and coefficients of temperature dependence of the density-of-state effective masses and energy gap width were taken from [17]. Electron scattering parameter  $r$  was considered to be equal to hole scattering parameter. With regard to the above, the density-of-state mass of holes was  $0.58(T/100)^{0.5}m_e$ , the density-of-state mass of electrons was  $0.5(T/100)^{0.35}m_e$ .

The Fermi level was found from the solution of neutrality equation

$$n_p - n_n = n, \quad (9)$$

where  $n_p$  – hole concentration,  $n_n$  – electron concentration. ThermoEMF for single-crystal grains was found from

$$\alpha_{n,p} = \frac{k}{e} \left[ \frac{(2r+5)F_{r+3/2}(\mu_{n,p}^*)}{(2r+3)F_{r+1/2}(\mu_{n,p}^*)} - \mu_{n,p}^* \right], \quad (10)$$

where  $k$  – the Boltzmann constant,  $e$  – electron charge,  $r$  – scattering parameter,  $F_n$  – the Fermi integrals,  $F_n(\mu^*) = \int_0^\infty \frac{x^n}{1 + \exp(x - \mu^*)} dx$ ,  $\mu_{n,p}^*$  – reduced Fermi level for electrons and holes. Indexes

$n$  and  $p$  denote electron or hole component. In the accepted approximations, the hole and electron components of thermoEMF are isotropic, but total thermoEMF in the region of mixed conduction can be anisotropic. A relation between the effective values of thermoEMF in a compacted polycrystalline sample and in single-crystal grains in the framework of model (2) and (3) is given by the ratios

$$\alpha_{ep\perp} = \frac{\alpha_{p\perp}\sigma_{p\perp}(2+t) + \alpha_{p\parallel}\sigma_{p\parallel}(1-t)}{3\sigma_{ep\perp}}, \quad (11)$$

$$\alpha_{ep\parallel} = \frac{2\alpha_{p\perp}\sigma_{p\perp}(1-t) + \alpha_{p\parallel}\sigma_{p\parallel}(1+2t)}{3\sigma_{ep\parallel}}, \quad (12)$$

where  $\alpha_{p\perp}$ ,  $\alpha_{p\parallel}$  – thermoEMF values in individual grains.

The resulting calculated temperature dependences of thermoEMF are represented in Fig. 1 and testify to their reasonable agreement with the experimental data. In the investigated temperature range a divergence between calculated values  $\alpha_{ep\perp}$  and  $\alpha_{ep\parallel}$  appears only at temperatures above 350 °C and does not exceed 1 – 2 μV/K. Experimental data (Fig. 1) also testify to the presence of small thermoEMF anisotropy (about 2 %) in compacted samples. Its emergence can be related to the effect of charge carrier scattering anisotropy on the grain boundaries. Electric conductivity anisotropy in a single crystal is also related to anisotropy of charge carrier mean free paths  $K_{p\sigma}$ . With a motion of charge carriers in a single grain of polycrystalline material for a direction perpendicular to trigonal axis, the mean free path is larger than for a parallel direction. Therefore, scattering processes on the grain boundaries will be more pronounced for a direction perpendicular to trigonal axis, which in the

presence of texture will result in the effective thermoEMF anisotropy for compacted material. However, this effect per se is very small and cannot result in considerable change of electric conductivity value, so determination of  $t$  without regard to scattering on grain boundaries can be considered to be sufficiently correct.

Relations of the type (2) and (3), with replacement  $\sigma$  by  $\kappa$  are also true for thermal conductivity. Based on them, with regard to texture coefficient, determined from the results of electric conductivity measurement, one can calculate thermal conductivity, parallel and perpendicular to triad axis in a single-crystal grain. Knowledge of band structure parameters allows calculating the electron component of thermal conductivity  $\kappa_{el}$  by the formulae [17]

$$\kappa_{el} = T \left( \frac{k}{e} \right)^2 \left\{ A_n \sigma_n + A_p \sigma_p + \frac{\sigma_n \sigma_p}{\sigma_n + \sigma_p} \left[ \delta_n + \delta_p + \frac{E_g}{kT} \right] \right\}, \quad (13)$$

$$A_{n,p} = \left[ \frac{(r+7/2) F_{r+5/2}(\mu_{n,p}^*)}{(r+3/2) F_{r+1/2}(\mu_{n,p}^*)} - \frac{(r+5/2)^2 F_{r+3/2}^2(\mu_{n,p}^*)}{(r+3/2)^2 F_{r+1/2}^2(\mu_{n,p}^*)} \right], \quad (14)$$

$$\delta_{n,p} = \left[ \frac{(r+5/2) F_{r+3/2}(\mu_{n,p}^*)}{(r+3/2) F_{r+1/2}(\mu_{n,p}^*)} \right], \quad (15)$$

where  $T$  – temperature,  $E_g$  – energy gap width,  $\sigma_n$  and  $\sigma_p$  are used to mean the respective values of electric conductivity in a direction perpendicular and parallel to trigonal axis [18]. The first two terms in braces (13) characterize the electron and hole contribution to thermal conductivity, the last term is a bipolar thermal conductivity.

To make full calculation of thermal conductivity, as it was done for thermoEMF, does not seem possible due to absence of data on the lattice thermal conductivity for single crystals of given composition. Therefore, one can only calculate the lattice thermal conductivity in a single-crystal grain for extrinsic conductivity region, where electron contribution to thermal conductivity can be neglected. According to the results of calculation for a single grain, the lattice thermal conductivity parallel to trigonal axis has a conventional temperature dependence  $\kappa_{L_1} \sim 1/T$ , as illustrated in Fig. 2.

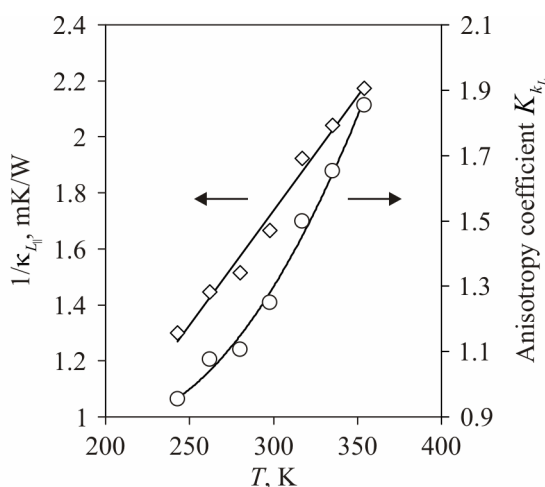


Fig. 2. Temperature dependence of lattice thermal conductivity in a single grain for a direction parallel to trigonal axis, and lattice conductivity anisotropy coefficient.

At the same time, the lattice thermal conductivity, perpendicular to trigonal axis, grows with a rise in temperature, as a result of which anisotropy coefficient  $K_{k_L} = \kappa_{L_\perp} / \kappa_{L_\parallel}$  also grows with temperature (Fig. 2). Such a difference in thermal conductivity mechanisms along and across trigonal axis is hard to explain in the framework of scattering inside a grain. Most probably it is related not to intragranular properties, but to phonon scattering on grain boundaries. The mean free path of phonons inside a grain is larger for a direction perpendicular to trigonal axis. Therefore, for this direction scattering on grain boundaries will be more pronounced. With temperature reduction, the mean free path of phonons is increased and scattering on grain boundaries will be more pronounced, resulting in equalization of mean free paths (and, as a consequence, of thermal conductivity) along the directions parallel and perpendicular to triad axis.

Approximation of thermal conductivity anisotropy coefficient to electric conductivity anisotropy coefficient (Fig. 1) will contribute to  $Z$  increase with a rise in temperature, since in a polycrystalline sample it will reduce the eddy currents caused by different ways for heat flux and electric current.

From (9) it is seen that a crucial factor in bipolar thermal conductivity in *p*-type semiconductor at the initial stage, when  $\sigma_p \gg \sigma_n$ , is electron conductivity. In single-crystal material the ratio of electron and hole mobilities depends on crystallographic orientation. For a direction perpendicular to triad axis the bipolar thermal conductivity is higher than the respective value for a parallel direction. In compacted material with texture this yields that in a direction perpendicular to compaction axis thermal conductivity, with a rise in temperature, grows faster, as a result of which thermoelectric figure of merit drops faster than for a parallel direction. This accounts for intersection of thermoelectric figure of merit curves for parallel and perpendicular directions at temperatures close to 320 K (Fig. 1). Calculation of a bipolar thermal conductivity component shows that at a temperature of 415 K in a perpendicular direction  $\kappa_{bip\perp} = 0.208$  W/m·K, and  $\kappa_{bip\parallel} = 0.059$  W/m·K.

The above regularities of influence of SPS conditions on the anisotropy of thermoelectric properties are also observed with separate measurement of  $\sigma$ ,  $\alpha$ ,  $\kappa$ . Fig. 3 represents the temperature dependences of thermoelectric properties measured by this method and the respective anisotropy coefficients for samples obtained by SPS method at a pressure of 30 MPa and 500 °C.

For SPS conditions 30 MPa and 500 °C at room temperature ( $\sim 297$  K),  $K_{ep\sigma}$  and  $K_{ep\kappa}$  are lower than in the samples obtained at 50 MPa and 450 °C (Fig. 1). The observed difference in temperatures corresponding to maximum  $ZT$  and intersection of curves  $ZT_\perp$  and  $ZT_\parallel$ , in Figs. 1 and 3, is also apparently related to the difference in sample sintering conditions. At the same time, it should be noted that, as is evident from Fig.3, when measuring  $D_t$  by laser flash method the differences in the values  $\kappa_{e\perp}$  and  $\kappa_{e\parallel}$  and appropriately calculated  $ZT_\perp$  and  $ZT_\parallel$  are within the accuracy of experimental procedure.

In this connection, we draw attention to another important feature of temperature diffusivity measurement procedure with the use of the LFA installation. As mentioned above, in this case the measured samples shaped as thin plates should have dimensions  $10 \times 10$  mm<sup>2</sup> or diameter 12 mm, and measurement is performed in a direction perpendicular to the surface of samples. In the majority of cases, including the works reporting very high values of  $ZT > 1.3$ , hot-pressed or spark plasma sintered samples shaped as pellets 2 – 3 mm thick are employed. Of such pellets one can cut out samples of necessary size for measuring  $D_t$  only perpendicular to compaction axis, and perform measurements along the compaction axis. This brings about a situation when  $\kappa_{e\parallel}$  and  $\sigma_{e\perp}$ ,  $\alpha_{e\perp}$  are measured in different directions, which results in considerable overrating of thermoelectric figure of merit value.

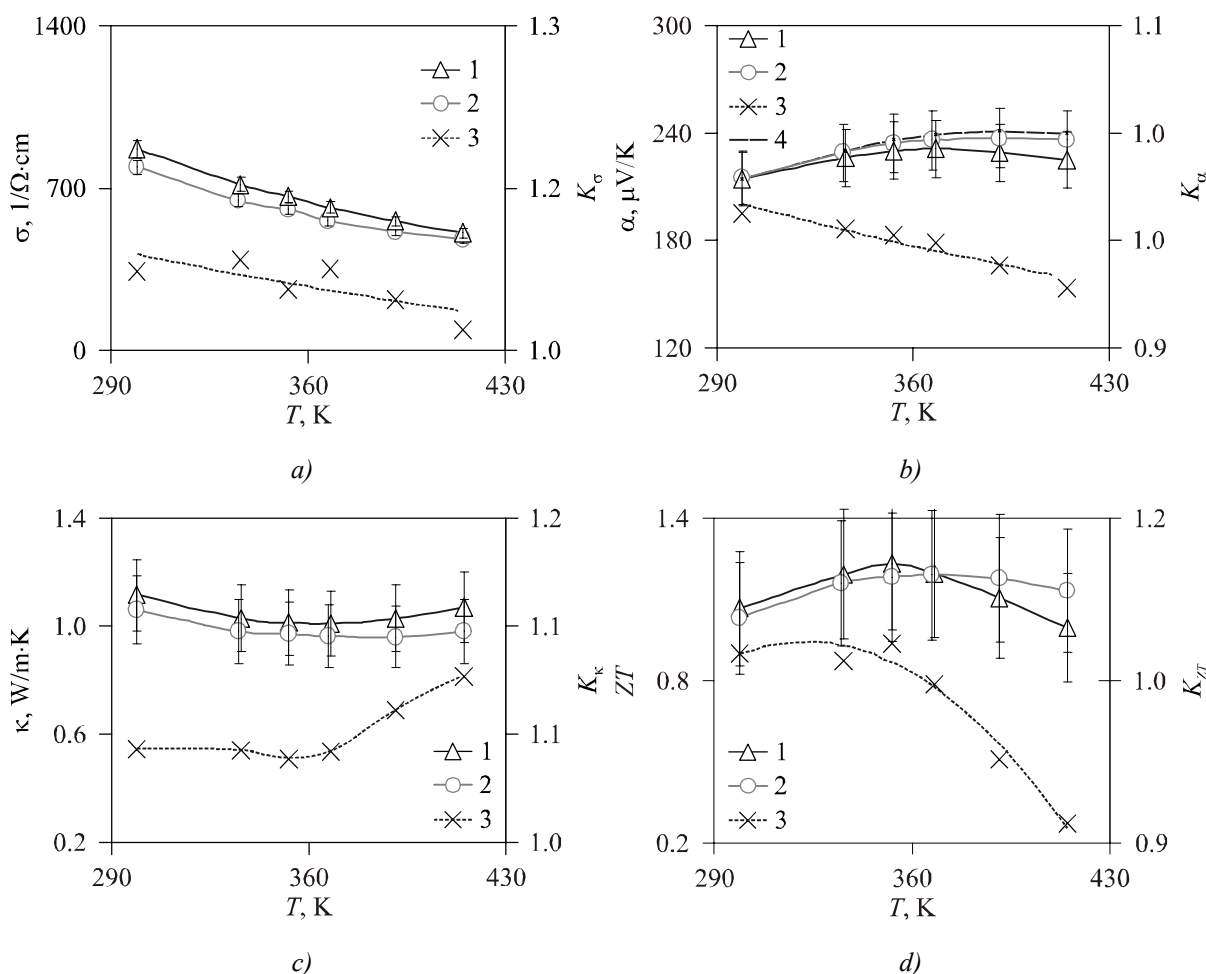


Fig. 3. Temperature dependences of electric conductivity (a), thermoEMF (b), thermal conductivity (c), dimensionless thermoelectric figure of merit (d) of  $\text{Bi}_{0.4}\text{Sb}_{1.6}\text{Te}_3$  samples obtained by SPS method at a pressure of 30 MPa, temperature 500 °C.

Method of separate measurement: 1 – perpendicular to compaction axis, 2 – parallel to compaction axis, 3 – anisotropy coefficient, 4 – results of thermoEMF calculation.

For instance, in [3], where for a textured pellet 13 mm thick, obtained by SPS method in the mode of 50 MPa, 380 °C, when  $\sigma_{\perp}$  and  $\kappa_{\parallel}$  are measured in different directions,  $ZT \sim 1.7$ , and when  $\sigma_{e\perp}$  and  $\kappa_{e\perp}$  are measured in the same direction,  $ZT \sim 1.1$ .

Therefore, the values of  $ZT > 1.3$  obtained on thin samples without regard to anisotropy give rise to doubt.

## Conclusions

Anisotropy of thermoelectric properties of *p*-type nanostructured  $\text{Bi}_{0.4}\text{Sb}_{1.6}\text{Te}_3$  material obtained by spark plasma sintering method (SPS) has been studied as a function of compaction pressure and temperature. Unlike the majority of works, the thermoelectric properties were determined both by Harman's method and the method of separate measurement of electric conductivity  $\sigma$ , thermoEMF  $\alpha$  and thermal conductivity  $\kappa$  on different samples. In a direction perpendicular to compaction axis,  $\sigma_{\perp}$  and  $\kappa_{\perp}$  are higher than in a direction parallel to  $\sigma_{\parallel}$  and  $\kappa_{\parallel}$ . It has been established that electric conductivity anisotropy exceeds thermal conductivity anisotropy. The values of anisotropy

coefficients  $K_\sigma$  and  $K_\kappa$  increase with SPS pressure increase and temperature reduction. From the experimental values of electric and thermal conductivity in various directions coefficients of texture in compacted material have been calculated. The resulting calculated temperature dependences of thermoEMF are in reasonable agreement with the experimental data. For a single-crystal grain in the extrinsic conduction region the results of calculation of the temperature dependence of lattice thermal conductivity in perpendicular and parallel directions with respect to trigonal axis have been given. Starting from certain temperature depending on sample preparation conditions, the value of thermoelectric figure of merit  $ZT$  in a direction parallel to compaction axis becomes larger than in the perpendicular direction, which is due to the emergence of minor carriers and the difference in hole and electron mobility ratios in single-crystal material for directions parallel and perpendicular to trigonal axis. Comparison of the errors in determination of thermoelectric material parameters with Harman's method and the method of separate measurement of electric conductivity, thermoEMF and thermal conductivity on different samples has been made. In the latter case high values of  $ZT > 1.3$  obtained on thin samples without regard to anisotropy, can be overrated due to specificity of temperature diffusivity measurement by laser flash method.

## References

1. B. Poudel, Q. Hao, Y. Ma, X.Y. Lan, A. Minnich, B. Yu, X. Yan, D.Z. Wang, A. Muto, D. Vashaee, X.Y. Chen, J.M. Liu, M.S. Dresselhaus, G. Chen, and Z.F. Ren, High-Thermoelectric Performance of Nanostructured Bismuth Antimony Telluride Bulk Alloys, *Science* **320** (5876), 634 (2008).
2. Experimental Studies on Anisotropic Thermoelectric Properties and Structures of n-type  $Bi_2Te_{2.7}Se_{0.3}$ , *Nano Letters* **10**, 3373 (2010).
3. J. Shen, L.P. Hu, T.J. Zhu, and X.B. Zhao, The Texture Related Anisotropy of Thermoelectric Properties in Bismuth Telluride Based Polycrystalline Alloys, *Appl. Phys. Lett.* **99** (124102), 356 (2011).
4. D.H. Kim, C. Kim, S.H. Heo, and H. Kim, Influence of Powder Morphology on Thermoelectric Anisotropy of Spark-Plasma-Sintered  $Bi-Te$ -based Thermoelectric Materials, *ScienceDirect*. **59** (5), 405 (2011).
5. V.T. Bublik, D.I. Bogomolov, Z.M. Dashevsky et al., Comparison of Structure of Thermoelectric Material  $Bi_{0.5}Sb_{1.6}Te_3$  Prepared by Hot Pressing and Spark Plasma Sintering Methods, *Izvestiya VUZov. Materialy Elektronnoi Tekhniki* **2**, 61 – 65 (2010).
6. V.N. Abrutin, I.A. Drabkin, I.I. Maronchuk, and V.B. Osvenski, Measurement of Thermoelectric Samples by Harman Method, IX Interstate Workshop Thermoelectrics and Their Applications (Saint-Petersburg, A.F.Ioffe FTI of RAS, 2004), P.303.
7. V. Abrutin, I. Drabkin, and V. Osvenski, Corrections Used when Measuring Thermoelectric Properties by Harman method, *Proc. 2<sup>nd</sup> Conference on Thermoelectrics* (Krakov, 2004), P.4.
8. W. Xie, J. He, S. Zhu, T. Holgate, S. Wang, X. Tang, Q. Zhang, and T. Tritt, Investigation of the Sintering Pressure and Thermal Conductivity Anisotropy of Melt-Spun Spark-Plasma-Sintered  $(Bi, Sb)_2Te_3$  Thermoelectric Materials, *J. Mater. Res.* **26** (15), 2143 (2011).
9. O. Madelung, U. Rössler, and M. Schulz (ed.), Collaboration: Authors and editors. The Landolt-Börnstein Database, *Springer Materials* (<http://www.springermaterials.com>) **41C** (3), 17E-17F (1998).
10. V.I. Odelevsky, Calculation of Generalized Conductivity of Heterogeneous Mixtures, *Technical Physics* **21**, 1379 (1951).

11. D. Stroud, Generalized Effective Medium Theory for the Conductivity of an Inhomogeneous Medium, *Phys. Rev. B* **112** (8), 3368 (1975).
12. Xia Ting-Kang, D. Stroud, Theory of the Hall Coefficient of Polycrystals: Application to a Simple Model for  $La_{2-x}M_xCuO_4$  ( $M = Sr, Ba$ ), *Phys. Rev. B* **37** (1), 119 (1988).
13. G.N. Dulnev, Yu.P. Zarichniak, Thermal Conductivity of Mixtures and Composite Materials. Handbook (Leningrad: Energia, 1974), 264 p.
14. V.T. Bublik, Z.M. Dashevsky, I.A. Drabkin, et al., Transport Properties in the Temperature Range 190 – 300 K of Nanostructured  $p$ - $Bi_{0.5}Sb_{1.5}Te_3$  Prepared by Spark Plasma Sintering Technique (Saint-Petersburg, Thermoelectrics and Their Applications, 2010), 47 p.
15. L.N. Lukyanova, V.A. Kutasov, P.P. Konstantinov, and V.V. Popov, Thermoelectric Figure of merit in  $p$ -type Solid Solutions Based on Bismuth and Antimony Chalcogenides at Higher than Room Temperatures, *Physics of The Solid State* **52** (8), 1492 (2010).
16. M. Stordeur, M. Srölzer, H. Sobottam, and V. Rieder, Investigation of the Valence Band Structure of Thermoelectric  $(Bi_{1-x}Sb_x)Te_3$  Single Crystals, *Phys. Stat. Sol. (b)* **150** (1), 150 (1988).
17. M.K. Zhitinskaya, V.I. Kaidanov, and V.P. Kondratyev, ThermoEMF Anisotropy in Bismuth Telluride Single Crystals, *Semiconductors* **10** (11), 2185 (1976).
18. I.A. Smirnov, V.I. Tamarchenko, *Electron Thermal Conductivity in Metals and Semiconductors* (Leningrad: Nauka, 1977), 151 p.

Submitted 22.04.2013.